Author's response to Referee 1

1. **Comments from the Anonymous Referee 1**
   - In the introduction section it is mentioned that the LRI data also provide information on attitude (pitch and yaw). I am not sure if this data is used/provided in the nominal GRACE-FO SDS Level-1B data processing. Some background information should be given.

   Author's response
   The following sentence was added in page 2: Therefore GRACE-FO LRI data processing will contain precise measurements of the satellites' pitch and yaw angles.

2. **Comments from the Anonymous Referee 1**
   Same section: The authors mentioned Kim (2000) as a realistic pre-launch simulation of GRACE but forgot to mention Flechtner et al. (2016): What Can be Expected from the GRACE-FO Laser Ranging Interferometer for Earth Science Applications? - Surveys in Geophysics, 37, 2, p. 453-470. http://doi.org/10.1007/s10712-015-9338-y. Also here a simulation of the possible impact of the LRI on the GRACE-FO gravity field results and various applications is performed. In this paper 5 years of realistic instrument data and background model errors have been simulated (but not been made public).

   Author's response
   The following sentence was added in page 1: Flechtner et al. (2016) have performed a full-scale simulation over the nominal GRACE-FO mission lifetime of 5 years and showed notable improvements with the LRI, on a global scale, of the order of 23%.

3. **Comments from the Anonymous Referee 1**
   Also a hint to the plans of the GRACE-FO Science Data System to provide a set of simulated GRACE-FO data to the user community within the so called ?Grand Simulation? shall be mentioned. E.g. taking the GRACE-FO status reports / abstracts of presentations in Kobe (IUGG) or Vienna (EGU). Nevertheless, it has to be mentioned that this activity is much behind schedule and therefore the provided data set is very useful to start just now!
   Author's response
   The following sentence was added in page 1: Also, GRACE-FO science data system team at Jet Propulsion Laboratory (JPL) has planned to release a GRACE-FO "Grand Simulation" data set before the real GRACE-FO data is available (Watkins et al., 2016).

4. **Comments from the Anonymous Referee 1**
   - It is not 100% clear what the time period of the simulated data is. I assume (without check by downloading the data) that it is one month. There are also later sentences such as ?we simulated one month of data?. This general information should be given at the very beginning.

   Author's response
   At page 2, line 6 in the **Introduction**, the duration of the simulated data has already been mentioned:
   'We have generated a set of simulated GRACE-FO data for the period of one month.'

5. **Comments from the Anonymous Referee 1**
   If it is just a month then analysis of trends or seasonal/sub-seasonal signals are not in the focus, but more a check if the simulated data can be read by the processing centers and how good the recovered field fits to the gravity field used for simulation. This points to question b) in the general comments. Should be discussed.
   Author's response
   The following paragraph was added in page 2: We have generated a set of simulated GRACE-FO data for a period of one month with 5-second sampling rate. A brief overview about the scope of the simulations are given in Naeimi et al. (2017).

The data set is available for download via https://doi.org/10.22027/AMDC2. The recovered gravity field solutions using this data set can be submitted via the same link. Therefore the goal of generating this set of simulated data are:

- Improving different gravity field recovery techniques, by comparing the input gravity field for the simulation and the recovered gravity fields
- Using new LRI data such as LRI ranging and LRI attitude information in different gravity field recovery techniques

The analysis of seasonal or sub-seasonal geophysical features are not the focus of this simulated data set, as the duration of the simulated data is short.

6. **Comments from the Anonymous Referee 1**
   - Also I suggest that the authors provide some results at the end that they were successful with their own software (if existing?) to recover the noise-free and noisy data with such and such error (e.g. by degree variance plots). This would be close-loop verification before external users test the data.
   Author's response
   We did a close-loop verification. But as we mentioned in the introduction, the main scope of this paper is describing how the simulated data was generated. We will address the gravity field recovery from this set of simulated data by different approaches in a future paper.

7. **Comments from the Anonymous Referee 1**
   Page 3, Line 14: . . .and a GPS error is added to each. . .: see comment below for KBR and SCA
   Author's response
   The following sentence was added in page 3: the following sections in this paper describe each simulated instrument observations and errors respectively:

8. **Comments from the Anonymous Referee 1**
   - Page 3, Line 16: . . .with added KBR errors. . .: I think here it should be already mentioned what is included in the error budget or at least a clear statement that the errors are all discussed in chapter 6.
   Author's response
   The following sentence was added in page 3: the following sections in this paper describe each simulated instrument observations and errors respectively:

9. **Comments from the Anonymous Referee 1**
   - Page 4, Line 2: similar comment for the SCA1B errors
   Author's response
   The following sentence was added in page 3: the following sections in this paper describe each simulated instrument observations and errors respectively:

10. **Comments from the Anonymous Referee 1**
    - Page 4, Line 3: For the Accelerometer data it looks like if they do not contain errors (but have as shown in Figure 2 and discussed later)
    Author's response
    The following sentence was added in page 4: Then accelerometer noise, scale and bias are added.

11. **Comments from the Anonymous Referee 1**
    - Page 4, Line 7: same comment as for KBR1B
    Author's response
    The following sentence was added in page 3: the following sections in this paper describe each simulated instrument observations and errors respectively:

12. **Comments from the Anonymous Referee 1**
    - Page 4, Figure 2: Imprecise, as quaternions here do not contain errors

Author's response

The following sentence was added in Figure 2's label: please refer to Fig. 6 for detailed description on SCA simulated data

13. **Comments from the Anonymous Referee 1**

Page 5, Line 11: Don't understand ?a static gravity field of d/o between 75 and 90?. What has been used for simulation? Is this description a hint what is stated in line 18 namely that the user shall try to solve for the right degree and order which fits best to the simulated field? I would more expect that they used a fixed degree and order (e.g. 90) with coefficients which are unknown to the user and provide this max d/o to the user.

Author's response

The sentence was changed into: 'A static gravity field of a certain degree and order.' and the following sentence was added in page 6: 'The degree and order that was used as input are between 75 and 95.'

14. **Comments from the Anonymous Referee 1**

Page 5, Line 10: It should be discussed that other gravitational forces such as atmosphere and ocean short term mass variations or an ocean pole tide model are not used (for simplicity) and this simulation data set focuses on impact of instrument data errors.

Author's response

The following sentence was added in page 6: Other gravitational forces such as atmosphere and ocean short term mass variations are not used as this simulation data set focuses on impact of instrument data errors.

15. **Comments from the Anonymous Referee 1**

Page 5, Line 12/13: Reference for eot11a and DE405 missing

Author's response

The references, (Rieser et al., 2012) and (Standish, 1998) were added.

16. **Comments from the Anonymous Referee 1**

Page 6, Line 1ff: information on used altitude, eccentricity and inclination missing, also on length of the simulation (1 month?)

Author's response

This information were added in Table 1.

17. **Comments from the Anonymous Referee 1**

- Page 7, Line 12: Would be good to know (and also the reference) how large the GRACE noise level is for RPY angles.

Author's response

Th following sentence and Figure 4 were added in page 8: The GRACE star cameras are strong in the roll axis and weak in the pitch and yaw axes due to the orientation in which they were mounted (cf. Harvey, 2016). GRACE data (Fig.4) confirms $150 - 300 \frac{\mu\text{rad}}{\sqrt{\text{Hz}}}$ accuracy for pitch and yaw, and $25 - 35 \frac{\mu\text{rad}}{\sqrt{\text{Hz}}}$ for roll, which meets the mission requirements (cf. Stanton, 1998).

18. **Comments from the Anonymous Referee 1**

- Page 10, Line 6: The authors mentioned ACC biases and scales. The value of the bias is known from Horwath et al (2011), but the values chosen for the scale factors are not known to the user. Some lines below it is only mentioned that certain constant values for each axis were chosen. As both have to be adjusted during gravity field determination it would be interesting to compare the simulated and adjusted values. The authors should mention if these scale factors will be made available.

Author's response

The following sentence was added in page 11: The scale and bias parameters will be available via https://doi.org/10. 22027/AMDC2 for comparison with the estimated ones.

19. **Comments from the Anonymous Referee 1**

- Page 10, Line 12ff: Here a first hint is given that one month of data was simulated (see comments above)

Author's response

This was addressed in item 4.

20. **Comments from the Anonymous Referee 1**

Page 22, Line 2: This statement is not complete as the quality of GRACE-FO models also depends on knowledge of short-term tidal and non-tidal mass variations (which have also large influence on the adjusted gravity model; in contrast to Flechtner et al. was not simulated). Nevertheless, it is highly appreciated that such a well described set of simulated GRACE-FO instrument data is now being available to the different gravity field processing centers.

Author's response

The sentence was changed into: We have described the simulation of observation and noise models for GRACE-FO multi-sensor system, consisting of inter-satellite ranging with microwave and laser ranging instrument, GPS orbit tracking, accelerometry, and attitude sensing.

21. **Comments from the Anonymous Referee 1**

Page 6, Line 19: More importantly, even though the KBR will be the primary science instrument and the LRI, a technology demonstrator, a threshold: This sentence shall likely read: More importantly, even though the KBR will be the primary science instrument, for the LRI, a technology demonstrator, a threshold of. . .

Author's response

The sentence was changed accordingly:

22. **Comments from the Anonymous Referee 1**

- Page 11, Line 11: As the abbreviation is δ_{SO} I suggest to write . . .is dominated by system and oscillator noise. . .

Author's response

The sentence was changed accordingly:

23. **Comments from the Anonymous Referee 1**

- Page 20, Line 9: Therefore, the angle determination is quantization limited shall read Therefore, the angle determination quantification is limited ? or?

Author's response

The sentence was changed into: However, the steering mirror can only turn in discrete units of 4.5μrad around the pitch axis and 6μrad around the yaw axis. Therefore, the angle determination is limited to integer multiples of these units.

Author's response to Referee 2

1. **Comments from the Anonymous Referee 2**

Page 2 line 6: Simulator data for period of one month. But, if Grace FO continues monthly summary data as per GRACE, don?t we need at least a two-month simulation to identify month-to-month variance of the monthly summaries?

Author's response

The following paragraph was added in page 2: Therefore the goal of generating this set of simulated data are:

– Improving different gravity field recovery techniques, by comparing the input gravity field for the simulation and the recovered gravity fields

– Using new LRI data such as LRI ranging and LRI attitude information in different gravity field recovery techniques

The analysis of seasonal or sub-seasonal geophysical features are not the focus of this simulated data set, as the duration of the simulated data is short.

2. **Comments from the Anonymous Referee 2**

Page 3 line 6: Why do we start with Figure 11 instead of Figure 1. This numbering remains a residual of originally

having two separate manuscripts?

Author's response

The Figure numbering is correct and starts from 1 in on-line PDF version.

3. **Comments from the Anonymous Referee 2**

Page 3 line 9: Here we find actual resolution, daily at 5 seconds. Helpful to have this information earlier?

Author's response

The following paragraph was added in page 2: We have generated a set of simulated GRACE-FO data for a period of one month with 5-second sampling rate.

4. **Comments from the Anonymous Referee 2**

Page 4, line 8: Table 11 (and subsequently tables 21 and 31) instead of Table 1, 2, 3?

Author's response

The Table numbering is correct and starts from 1 in on-line PDF version.

5. **Comments from the Anonymous Referee 2**

Comparing range, range rate and range acceleration noise predictions for KBR (Figure 17) and LRI (Figure 110) (AGAIN NOTE THE STRANGE NUMBERING SEQUENCE FOR FIGURES), (or likewise for time series in Figure 18 for KBR and Figure 112 for LRI) the authors suggest at least 2 order of magnitude lower noise, and in some cases perhaps better than 4 order of magnitude lower noise for the LRI. But this substantial improvement assumes, e.g. as described on page 5, that the laser ranging instrument pointing angle uncertainty - by engineering mechanism not yet solved - does not exceed some threshold which causes interferometry to fail (?falling out of lock?). The reader sees very hopeful numbers from this particular simulation but based on a very large assumption?

Author's response

We think that the paragraph in page 6 lines 17 to 23 is misleading, so we reformulated it into:

An attitude and orbit control system keeps the satellite orientation near its nominal attitude, within a certain boundary for each of the three pointing angles. These boundaries have been lowered for GRACE-FO compared to GRACE for two reasons. Firstly, due to the coupling of pointing angle errors into the ranging data; experience has shown that improved pointing would enhance the quality of gravity field solutions (Horwath et al., 2011). Secondly, the LRI requires better satellite pointing, in order to guarantee its functionality; otherwise there is a risk that the laser beam starts to hit obstacles. Hence, the combined effect of pointing jitter on one hand and frame misalignments on the other hand, together, cannot exceed a certain value (of about a few milliradians in terms of pitch and yaw angles for GRACE-FO). This yields strict requirements for the construction and mounting of the LRI components, and also the necessity for an improved pointing control.

The pointing jitter angles describe how the 'true' satellite orientation (as it actually is) deviates from the 'nominal' orientation (as it should be ideally in the absence of pointing angles). The nominal orientation is satellites' attitude reference. We assumed the satellites' attitude reference is the alignment of SF and LOSF for the simulations.

6. **Comments from the Anonymous Referee 2**

The two-orbit (roughly 3 hour) plots (Figure 14, Figure 19, Figure 114, 115, 117) provide the reader / user with highest resolution examples of specific per-orbit angles or jitter as reproduced by the simulations. But users applying Level-1B processing / formatting will not usually see or consider this level of detail?

Author's response

Yes, but in this section we are referring to two references, Bandikova et al. (2012) and Horwath et al. (2011). In both, there are similar attitude information plots for three hours orbit. Accordingly, the following paragraph was added in page 8:

The value of bias for each angle was chosen in range of a few milliradians. This level of bias has investigated by Horwath

et al. (2011) based on GRACE Level-1B data. Fig. 5 shows simulated star camera roll, pitch and yaw angles, which are similar to the GRACE inter-satellite pointing variations plot in Bandikova et al. (2012).

Instrument Data Simulations for GRACE Follow-on: Observation and Noise Models

Neda Darbeheshti[1], Henry Wegener[1], Vitali Müller[1], Majid Naeimi[2], Gerhard Heinzel[1], and Martin Hewitson[1]

[1]Max Planck Institute for Gravitational Physics (Albert Einstein Institute)-Leibniz Universität Hannover
[2]Institut für Erdmessung-Leibniz Universität Hannover

Correspondence to: Neda Darbeheshti (neda.darbeheshti@aei.mpg.de)

Abstract. The Gravity Recovery and Climate Experiment (GRACE) mission has yielded data on the Earth's gravity field to monitor temporal changes for more than fifteen years now. The GRACE twin satellites use microwave ranging with micrometer precision to measure distance variations between two satellites caused by the Earth's global gravitational field. GRACE Follow-on (GRACE-FO) will be the first satellite mission to use inter-satellite laser interferometry in space. The laser ranging instrument (LRI) will provide two additional measurements compared to the GRACE mission: interferometric inter-satellite ranging with nanometer precision and inter-satellite pointing information. We have designed a set of simulated GRACE-FO data, which include LRI measurements, apart from all other GRACE instrument data needed for the Earth's gravity field recovery. The simulated data files are publicly available via https://doi.org/10.22027/AMDC2 and can be used to derive gravity field solutions like from GRACE data. This paper describes the scientific basis and technical approaches used to simulate the GRACE-FO instrument data.

1 Introduction

The space gravimetry mission GRACE (Tapley et al., 2004) observes the Earth's gravity field changes with time. GRACE is the first low-low satellite-to-satellite tracking mission: the principal measurement is the distance variability between low orbit GRACE twin satellites which translates into the monthly gravity models (Wahr et al., 1998).

Kim (2000) published the first GRACE satellite simulation study before the launch of the GRACE satellites (in 2002). Now, seventeen years later, GRACE satellites are at the end of their lifetime and GRACE-FO data will be available soon. Although the GRACE-FO mission, and respectively its instrument data streams, will be very similar to GRACE, the necessity for GRACE-FO instrument data simulation emerges from the additional interferometric inter-satellite ranging. Flechtner et al. (2016) have performed a full-scale simulation over the nominal GRACE-FO mission lifetime of 5 years and showed notable improvements with the LRI, on a global scale, of the order of 23%. Also, GRACE-FO science data system team at Jet Propulsion Laboratory

(JPL) has planned to release a GRACE-FO "Grand Simulation" data set before the real GRACE-FO data is available (Watkins et al., 2016).

Most importantly, the operation of the LRI in addition to the primary K-band ranging (KBR) instrument yields extra information not only in the ranging measurement, but also in the attitude determination, since the LRI data stream . Therefore GRACE-FO LRI data processing will contain precise measurements of the satellites' pitch and yaw angles. In this paper for the first time, simulated LRI pitch and yaw angles are provided. Exploitation of the new GRACE-FO measurements has great potential to improve spatial and temporal resolution of the Earth's gravity field solutions.

Also, there are different techniques to recover the Earth's gravity field from GRACE-like data (e.g., Reigber (1989), Gerlach et al. (2003), Mayer-Gürr (2006) , Rummel (1979)). Therefore, simulated instrument data provide a controlled, closed form medium, to test and improve different gravity field recovery techniques.

We have generated a set of simulated GRACE-FO data for the a period of one month with 5-second sampling rate. A brief overview about the scope of the simulations are given in Naeimi et al. (2017). The data set is available for download via https://doi.org/10.22027/AMDC2. The recovered gravity field solutions using this data set can be submitted via the same link. Therefore the goal of generating this set of simulated data are:

– Improving different gravity field recovery techniques, by comparing the input gravity field for the simulation and the recovered gravity fields

– Using new LRI data such as LRI ranging and LRI attitude information in different gravity field recovery techniques

The analysis of seasonal or sub-seasonal geophysical features are not the focus of this simulated data set, as the duration of the simulated data is short.

The main purpose of this paper is to describe the chain of instrument data simulation procedure. The first section presents the preliminaries for the data simulation, including the coordinates systems and symbols, followed by each section describing each instrument data simulation, including details of instruments' noise models.

2   Preliminaries

The following coordinate systems are used to define the various simulated data:

International Celestial Reference Frame (ICRF) – Inertial frame:

– origin: center of mass (CoM) of the Earth

– axes: according to IERS 2010 conventions (Petit and Luzum, 2010)

International Terrestrial Reference Frame (ITRF) – Earth-fixed (co-rotating) frame:

– origin: CoM of the Earth

2

- axes: according to IERS 2010 conventions (Petit and Luzum, 2010)

line-of-sight frame (LOSF), one per satellite, for GRACE A:

- origin: satellite's CoM
- $x_{LOSF_A} = \frac{r_B - r_A}{|r_B - r_A|}$, where r is the satellites' position vector in the ICRF (i.e., line-of-sight vector and roll axis).
- $y_{LOSF_A} = \frac{x_{LOSF_A} \times r_A}{|x_{LOSF_A} \times r_A|}$ (i.e., pitch axis)
- $z_{LOSF_A} = x_{LOSF_A} \times y_{LOSF_A}$ (i.e., yaw axis)
  (for GRACE B, A and B indices should be exchanged.)

satellite frame (SF), one per satellite according to Case et al. (2002):

- origin: satellite's CoM
- $x_{SF} =$ from the origin to a target location of the phase center of the K/Ka band horn
- $y_{SF} =$ forms a right-handed triad with x_{SF} and z_{SF}
- $z_{SF} =$ normal to x_{SF} and to the plane of the main equipment platform, and positive towards the satellite radiator on the bottom of the GRACE-FO

The LOSF and SF are shown in Fig. 1. Since we did not model variations of the satellites' CoM (and the CoM coinciding with the on-board accelerometer's proof masses) for data simulation, the SF coincides with the science reference frame defined in Case et al. (2002).

All simulated data are published in GRACE Level-1B data format: daily files with 5-second sampling rate (cf. Case et al., 2002). They can be considered pre-processed like GRACE Level-1B data. Time tags are given in GRACE GPS seconds, i.e. seconds since epoch 2000-01-01, 12:00:00 (no leap seconds applied). Five instrument data types were simulated; the following sections in this paper describe each simulated instrument observations and errors respectively:

- GPS Navigation Data (GNV1B)
  Simulated GPS positions and velocities are the output of the orbit integrator, which are rotated from ICRF to ITRF, and a GPS error is added to each. The error-free positions can be considered a kinematic orbit.

- K-Band Ranging System (KBR1B)
  Simulated KBR ranging data is derived from the error-free GPS positions and velocities with added KBR errors.

- Star Camera (SCA1B)
  Simulated star camera quaternions are derived from the simulated roll, pitch and yaw angles with added errors.
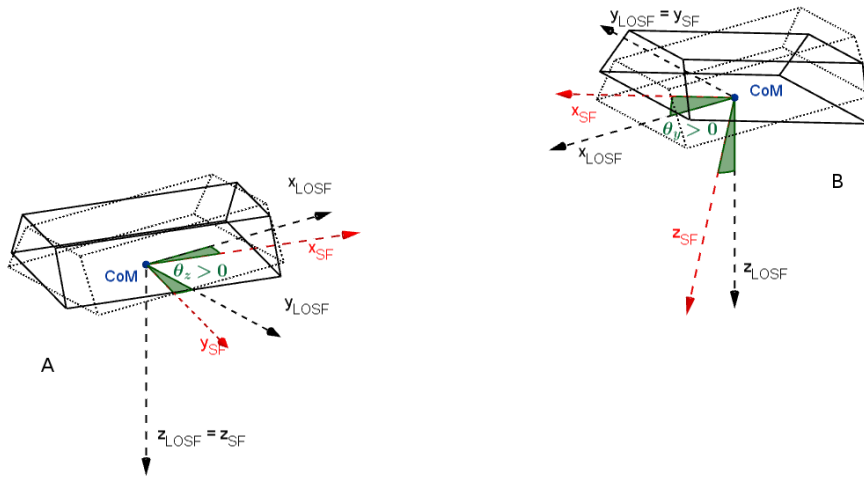
3

Figure 1. Illustration of SF and LOSF for GRACE satellites. Small positive yaw (left) and pitch (right) angles indicate the direction of rotation defining the sign of the pointing angles

- Accelerometer (ACC1B)

  Simulated linear accelerations are calculated from the non-gravitational accelerations acting on the satellites. The error-free simulated star camera quaternions are used to transform the linear accelerations from ICRF to SF. Then accelerometer noise, scale and bias are added. The angular accelerations are calculated from the error-free simulated star camera quaternions.

- Laser Ranging Instrument (LRI1B)

  Simulated LRI ranging data is derived from error-free GPS positions and velocities with added LRI errors.

Figure Fig. 2 shows a flowchart of the procedure used for the simulations. For each instrument, first the error-free observation was generated, and then the errors including instrument noise, bias and scale were applied to each instrument observation.

In this paper,

- The symbols δ and Δ are used for time-varying and constant errors, respectively.

- The symbol $\tilde{\delta}$ denotes amplitude spectral densities (ASD).

For data simulations,

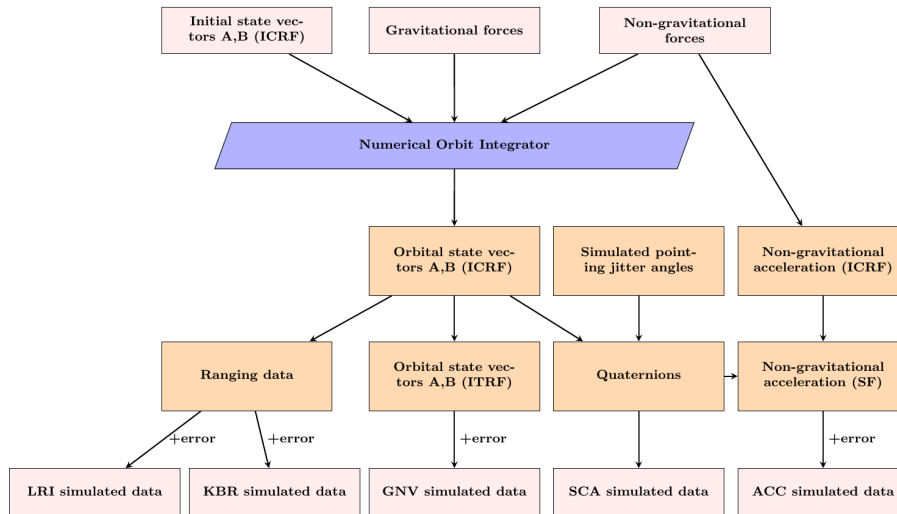- A five points numerical differentiation method was used for the numerical differentiations.

4

Figure 2. Flowchart of the simulation steps for GRACE-FO instrument data; please refer to Fig. 6 for detailed description on SCA simulated data

– The LISA Technology Package Data Analysis (LTPDA) toolbox (https://www.elisascience.org/ltpda/) for MATLAB was used for generation of time series based on instrument noise models given in terms of ASD. LTPDA uses Franklin's random noise generator method (Franklin, 1965) to generate arbitrarily long time series with a prescribed spectral density.

3 Simulating GNV1B Data

An orbit integrator is used to calculate the trajectories of the GRACE-FO satellites (GRACE-FO A and GRACE-FO B) by numerical integration of Newton's second law of motion, based on knowledge of the forces acting on the satellite. Table 1 summarises the orbit integrator parameters.

The IERS2010 conventions are used for rotation between the ITRF and the international celestial reference frame ICRF. Two types of force models were used for orbit integration:

Gravitational forces:

- A static gravity field of a certain degree and order~~between 75 and 95.~~.
- The Ocean tide model ~~(eot11a)~~ EOT11a (Rieser et al., 2012) up to degree and order 80.
- Direct tides of the Moon and Sun using NASA ~~Jet Propulsion Laboratory (JPL)~~ JPL DE405 ephemeris (Standish, 1998).
- Anelastic solid Earth tides according to IERS2010.

Non-gravitational forces:

5

Table 1. Orbit integrator parameters

Parameter	Description
Altitude	477.7 km
~~Numerical integration approach~~Eccentricity	~~Gauss-Jackson order 12~~ 0.0019
Inclination	$89.0081°$
~~Integration length~~ Numerical integration approach	~~31 days~~ Gauss-Jackson order 12
Integration length	31 days (May 2005)
Integration step size	5 seconds

- Atmospheric drag model

- Solar radiation pressure model

The static gravity model and its exact degree and order are the unknowns for the gravity field recovery. The degree and order that was used as input are between 75 and 95. The atmospheric drag and solar radiation pressure models are described in Appendix
5   A. Other gravitational forces such as atmosphere and ocean short term mass variations are not used as this simulation data set focuses on impact of instrument data errors.

The input to the orbit integrator is the initial time and state (position and velocity vectors) of GRACE-FO A and GRACE-FO B at time 00:00:00, 2005-05-01. It calculates the two trajectories separately, beside the time series of accelerations along the trajectory from the gravitational and non gravitational force models. The output of the orbit integrator are the time series of the
10   position, velocity and acceleration vectors of GRACE-FO A and GRACE-FO B:

$$\boldsymbol{r}_A, \quad \dot{\boldsymbol{r}}_A, \quad \ddot{\boldsymbol{r}}_A, \quad \boldsymbol{r}_B, \quad \dot{\boldsymbol{r}}_B, \quad \ddot{\boldsymbol{r}}_B$$

White noise with a level of a few $\frac{\mathrm{cm}}{\sqrt{\mathrm{Hz}}}$ was generated along x, y and z axes independently, and added to each satellite position:

$$\boldsymbol{r}_{GNV1B} = \boldsymbol{r} + \delta\boldsymbol{r}_{GNV1B} \tag{1}$$

15   Then the noise was differentiated numerically and added to the velocities along x, y and z axes separately for each satellite:

$$\dot{\boldsymbol{r}}_{GNV1B} = \dot{\boldsymbol{r}} + \delta\dot{\boldsymbol{r}}_{GNV1B} \tag{2}$$

4   Simulating SCA1B Data

The satellite attitude with respect to the ICRF is determined from the star cameras on board the satellites. The measured attitude is expressed in terms of quaternions q:

20   $$q = \begin{pmatrix} q_0 & q_1 & q_2 & q_3 \end{pmatrix} \tag{3}$$

Here, q_0 denotes the real component and q_1, q_2 and q_3 are the imaginary components of the quaternion. The time series of quaternions is provided in the SCA1B product.

~~In the GRACE satellites, an on-board attitude and orbital control system continuously attempts to align the pointing vector from the CoM to~~ An attitude and orbit control system keeps the satellite orientation near its nominal attitude, within a certain boundary for each of the three pointing angles. These boundaries have been lowered for GRACE-FO compared to GRACE for two reasons. Firstly, due to the ~~K-band antenna phase center (APC) with the line-of-sight vector, in order to keep the geometric error in the KBR measurement as small as possible. However~~ coupling of pointing angle errors into the ranging data; experience has shown that improved pointing would enhance the quality of gravity field solutions (Horwath et al., 2011). Secondly, the LRI ~~measurements are subject to a very similar effect. More importantly, even though the KBR will be the primary science instrument and~~ requires better satellite pointing, in order to guarantee its functionality; otherwise there is a risk that the laser beam starts to hit obstacles. Hence, the ~~LRI, a technology demonstrator, a threshold of some milliradians pointing variations may not be exceeded to prevent the laser interferometer from falling out of lock. To the authors' knowledge, it is not decided yet how this problem shall be addressed in the best way. For this reason, we assumed that~~ combined effect of pointing jitter on one hand and frame misalignments on the other hand, together, cannot exceed a certain value (of about a few milliradians in terms of pitch and yaw angles for GRACE-FO). This yields strict requirements for the construction and mounting of the LRI components, and also the necessity for an improved pointing control.

The pointing jitter angles describe how the 'true' satellite orientation (as it actually is) deviates from the 'nominal' orientation (as it should be ideally in the absence of pointing angles). The nominal orientation is satellites' attitude reference. We assumed the satellites' attitude reference is the alignment of SF and LOSF for the simulations.
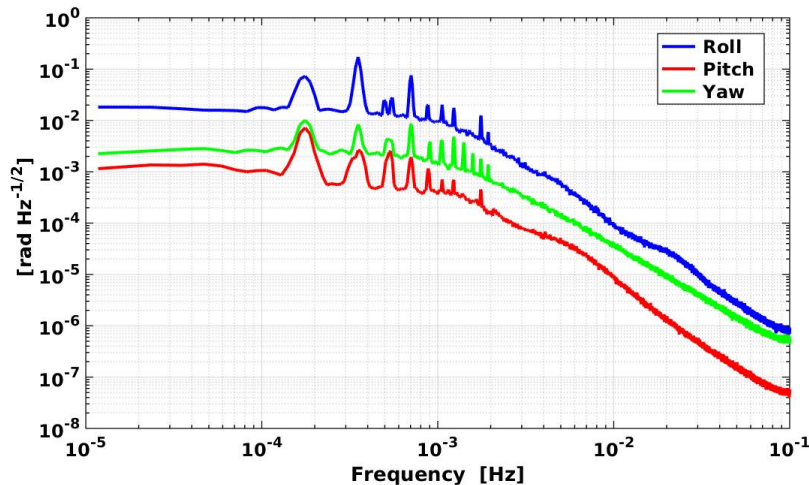

Figure 3. ASD of simulated roll, pitch and yaw angles

Accordingly, satellite pointing angles can be computed from star camera quaternions and orbital positions (described in Appendix B). For simulating star camera quaternions, one has to go the opposite way. Pointing angles from GRACE-FO attitude and orbital control system performance predictions were provided to us by JPL and AIRBUS Defense and Space. A model, which is based on the spectrum of these predicted angles, was used to simulate the pointing angles. The common
5 approach for generating time series with a known spectrum is to use a random noise generator. ~~Figure~~ Fig. 3 shows the ASD of the simulated roll (θ_x), pitch (θ_y) and yaw (θ_z) angles. One can see that all three angles have peaks mostly in the frequency band between 10^{-4} and $2 \cdot 10^{-3}$. These peaks disturb the functionality of the random noise generator, thus they were modelled individually. The result is a time series of error-free inter-satellite pointing angles.

To simulate star camera measurements, white noise ($\delta\theta_{SCA1B}$) and a bias ($\Delta\theta_{SCA1B}$) was added to each error-free angle
10 separately:

$$\theta_{x,SCA1B} = \theta_x + \delta\theta_{x,SCA1B} + \Delta\theta_{x,SCA1B}$$

$$\theta_{y,SCA1B} = \theta_y + \delta\theta_{y,SCA1B} + \Delta\theta_{y,SCA1B}$$

$$\theta_{z,SCA1B} = \theta_z + \delta\theta_{z,SCA1B} + \Delta\theta_{z,SCA1B} \tag{4}$$

Here, θ_x, θ_y and θ_z are the error-free simulated roll, pitch and yaw angles; $\theta_{x,SCA}$, $\theta_{y,SCA}$ and $\theta_{z,SCA}$ are simulated star camera roll, pitch and yaw angles.

The GRACE-FO satellites are equipped with improved star cameras compared to GRACE, and the number of star camera
15 heads will increase from two to three per satellite (Gath, 2016); also Bandikova et al. (2012) suggested that proper combination of the different star camera heads reduces high frequency noise of the pointing angles. Accordingly, it is expected that a better estimation of pointing angles from GRACE-FO star camera data will be available. Therefore, white noise with a level of a few ten $\frac{\mu\mathrm{rad}}{\sqrt{\mathrm{Hz}}}$ was chosen, which is lower than the current noise level in roll, pitch and yaw ~~angels~~ angles estimated from the GRACE star camera data. The GRACE star cameras are strong in the roll axis and weak in the pitch and yaw axes due to the
20 orientation in which they were mounted (cf. Harvey, 2016). GRACE data (Fig. 4) confirms $150 - 300 \frac{\mu\mathrm{rad}}{\sqrt{\mathrm{Hz}}}$ accuracy for pitch and yaw, and $25 - 35 \frac{\mu\mathrm{rad}}{\sqrt{\mathrm{Hz}}}$ for roll, which meets the mission requirements (cf. Stanton et al., 1998).

The value of bias for each angle was chosen in range of a few milliradians ~~(Horwath et al., 2011). Figure~~. This level of bias has investigated by Horwath et al. (2011) based on GRACE Level-1B data. Fig. 5 shows simulated star camera roll, pitch and yaw angles, which are similar to the GRACE inter-satellite pointing variations plot in Bandikova et al. (2012).

25 From the contaminated simulated pointing angles of equations (4), the rotation matrix $\mathbf{R}_{SF}^{LOSF}$ was built; and with the error-free simulated orbit positions, the rotation matrix $\mathbf{R}_{LOSF}^{ICRF}$ was built; having these two matrices, the matrix $\mathbf{R}_{SF}^{ICRF}$ is

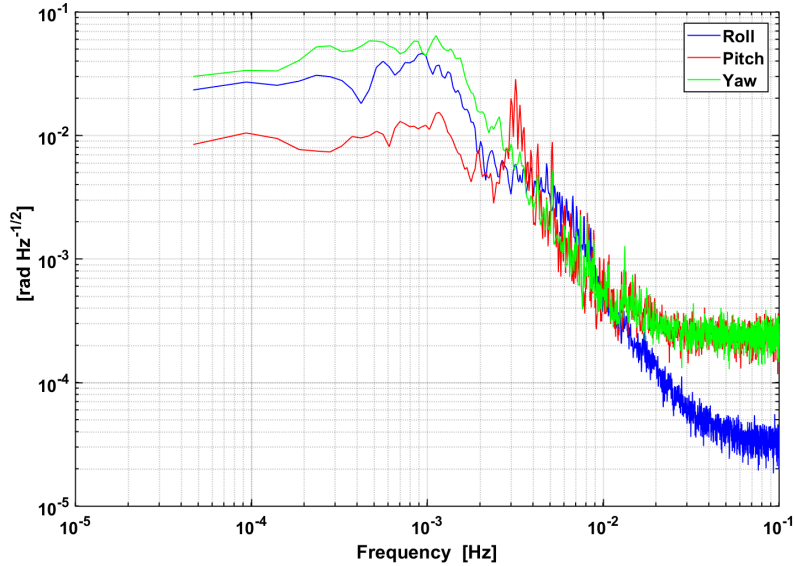$$\mathbf{R}_{SF}^{ICRF} = \mathbf{R}_{LOSF}^{ICRF} \cdot \mathbf{R}_{SF}^{LOSF}, \tag{5}$$

Figure 4. ASD of GRACE roll, pitch and yaw angles on 2008-12-01

containing the simulated star camera quaternions (cf. Fig. 6). Finally, the simulated quaternions can be recovered from the rotation matrix $\mathbf{R}_{SF}^{ICRF}$ by using the equations (Wu et al., 2006):

$$q_0 = \frac{1}{2}\sqrt{1 + R_{11} + R_{22} + R_{33}}$$
$$q_1 = \frac{(R_{23} - R_{32})}{4q_0}$$
$$q_2 = \frac{(R_{31} - R_{13})}{4q_0}$$
$$q_3 = \frac{(R_{12} - R_{21})}{4q_0} \tag{6}$$

where R_{ij} are the elements of $\mathbf{R}_{SF}^{ICRF}$. Note that the equations 6 are only numerically stable, as long as the trace of $\mathbf{R}$ is

5   non-negative (i.e. not close to -1). A numerically stable pseudocode that was used is shown in Appendix C.

Two other sets of quaternions were generated. Error-free quaternions from error-free pointing angles in equations (4); and noisy quaternions that come from white noise contaminated pointing angles without the bias. We will refer to these two set of quaternions in the following sections.

5   Simulating ACC1B Data

10   ~~Figure~~ Fig. 2 shows that the non-gravitational accelerations were computed along the orbit in ICRF.
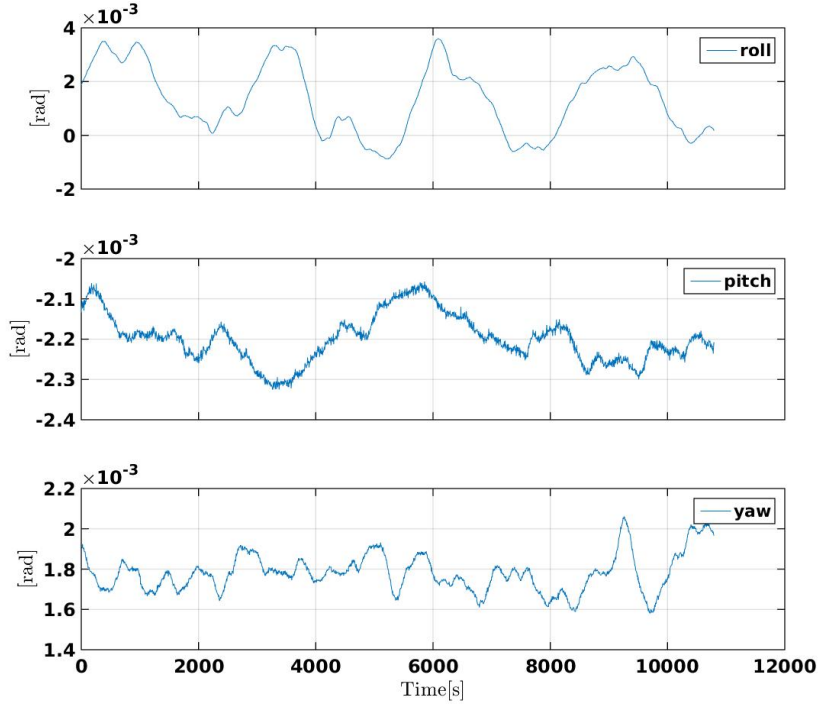
9

Figure 5. Simulated star camera roll, pitch and yaw angles during two orbital revolutions for GRACE-FO A

5.1 Linear Accelerations

The non-gravitational accelerations are the sum of atmospheric drag and solar radiation pressure accelerations (cf. Appendix A) along the orbit in inertial frame (ICRF). The non-gravitational accelerations $\ddot{\boldsymbol{r}}^{ICRF}$ were transformed into the satellite frame $\ddot{\boldsymbol{r}}^{SF}$ using the rotation matrix $\mathbf{R}^{SF}_{ICRF}$ from error-free simulated quaternions:

$$\ddot{\boldsymbol{r}}^{SF} = \mathbf{R}^{SF}_{ICRF} \cdot \ddot{\boldsymbol{r}}^{ICRF} \tag{7}$$

After being transformed into the SF, the linear accelerations were multiplied by the scale factors s_x, s_x and s_z, and then the accelerometer noise time series ($\delta\ddot{\boldsymbol{r}}_{ACC1B}$) and the biases ($\Delta\ddot{\boldsymbol{r}}_{ACC1B}$) were added along x, y and z axes independently:

$$\ddot{\boldsymbol{r}}^{SF}_{ACC1B} = \begin{bmatrix} s_x & 0 & 0 \\ 0 & s_y & 0 \\ 0 & 0 & s_z \end{bmatrix} \cdot \ddot{\boldsymbol{r}}^{SF} + \delta\ddot{\boldsymbol{r}}_{ACC1B} + \Delta\ddot{\boldsymbol{r}}_{ACC1B} \tag{8}$$
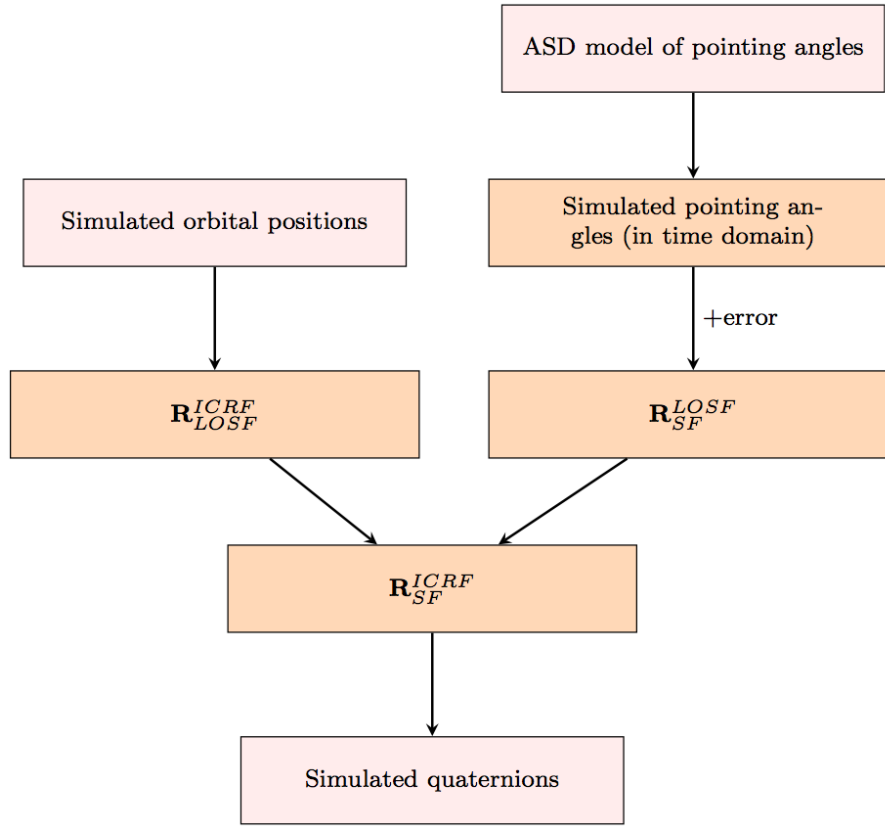
10

Figure 6. Flowchart of the simulation steps for SCA1B data

The ASD noise model of Kim (2000) was used to generate accelerometer noise ($\delta\ddot{\boldsymbol{r}}_{ACC1B}$):

$$\tilde{\delta\ddot{\boldsymbol{r}}}_{x/z,ACC1B}(f) = 10^{-10} \cdot \sqrt{1 + \frac{0.005\text{Hz}}{f}} \frac{\text{m/s}^2}{\sqrt{\text{Hz}}} \qquad 10^{-5} \leq f \leq 10^{-1}$$

$$\tilde{\delta\ddot{\boldsymbol{r}}}_{y,ACC1B}(f) = 10^{-9} \cdot \sqrt{1 + \frac{0.1\text{Hz}}{f}} \frac{\text{m/s}^2}{\sqrt{\text{Hz}}} \qquad 10^{-5} \leq f \leq 10^{-1}$$

(9)

The y axis in SF ($\boldsymbol{y}_{SF}$ in Fig. 1) is considered the least sensitive axis for accelerometer measurements (Kim, 2000). The noise ASD of the sensitive axes and the less sensitive axis are shown in Fig. 7. One month time series of the accelerometer noise was generated separately for x, y and z axes from the ASD models and added to the accelerations (equation (8)). Values close to GRACE accelerometer scale and bias along each axis were chosen, and kept constant for the one month of the simulated data. Therefore, in total for both satellites, six accelerometer scale parameters and six accelerometer bias parameters should be estimated during the gravity field recovery using one month of the simulated data. The scale and bias parameters will be available via https://doi.org/10.22027/AMDC2 for comparison with the estimated ones.
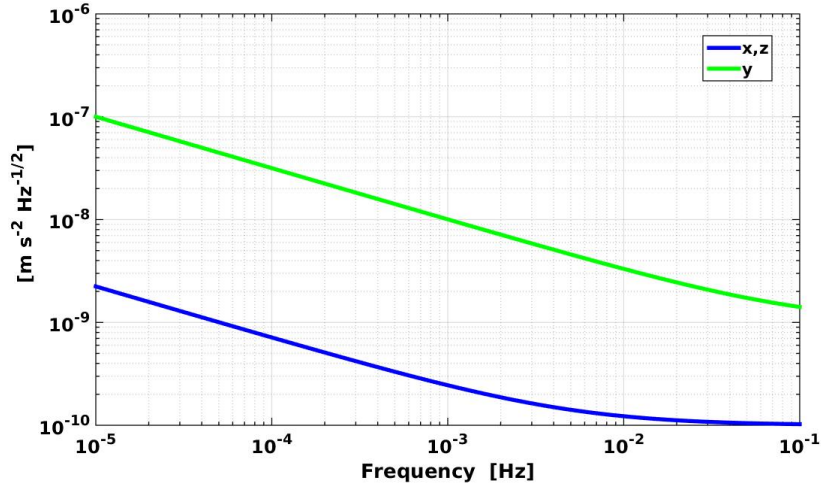
Figure 7. ASD of accelerometer noise

5.2 Angular Accelerations

The error-free simulated quaternions were used to generate angular accelerations, based on the relations between the quaternions and angular accelerations ($\dot{\omega}_x, \dot{\omega}_y, \dot{\omega}_z$) (cf. Müller, 2010):

$$
\begin{bmatrix} \dot{\omega}_x \\ \dot{\omega}_y \\ \dot{\omega}_z \\ -2\Sigma\dot{q}_m^2 \end{bmatrix} = 2 \cdot \begin{bmatrix} -q_1 & q_0 & q_3 & -q_2 \\ -q_2 & -q_3 & q_0 & q_1 \\ -q_3 & q_2 & -q_1 & q_0 \\ q_0 & q_1 & q_2 & q_3 \end{bmatrix} \cdot \begin{bmatrix} \ddot{q}_0 \\ \ddot{q}_1 \\ \ddot{q}_2 \\ \ddot{q}_3 \end{bmatrix}
$$

5 where $\ddot{q}_m$ are the numerically differentiated simulated quaternions.

6 Simulating KBR1B Data

The position, velocity and acceleration differences of GRACE-FO A and GRACE-FO B are calculated as follows:

$$\boldsymbol{r}_{AB} = \boldsymbol{r}_B - \boldsymbol{r}_A$$
$$\dot{\boldsymbol{r}}_{AB} = \dot{\boldsymbol{r}}_B - \dot{\boldsymbol{r}}_A$$
$$\ddot{\boldsymbol{r}}_{AB} = \ddot{\boldsymbol{r}}_B - \ddot{\boldsymbol{r}}_A, \tag{10}$$

in order to calculate simulated error-free range, range rate and range acceleration according to:

$$\rho = \sqrt{\boldsymbol{r}_{AB} \cdot \boldsymbol{r}_{AB}} \tag{11}$$

$$\dot{\rho} = \frac{\boldsymbol{r}_{AB}}{\rho} \cdot \dot{\boldsymbol{r}}_{AB} \tag{12}$$

$$\ddot{\rho} = -\frac{\dot{\rho}^2}{\rho} + \frac{\dot{\boldsymbol{r}}_{AB} \cdot \dot{\boldsymbol{r}}_{AB}}{\rho} + \frac{\boldsymbol{r}_{AB}}{\rho} \cdot \ddot{\boldsymbol{r}}_{AB} \tag{13}$$

5   where $\cdot$ is the vector dot product.

The GRACE-FO KBR instrument (as in GRACE) will measure the biased range between the twin satellites; respectively, a bias ($\Delta\rho$) of a few centimeters was added to the error-free range (ρ). The KBR instrument noise is dominated by ~~oscillator and system~~ system and oscillator noise ($\delta\rho_{SO}$). It was added to the error-free ranging products, as well as a geometric error, which is a pointing jitter coupling effect caused by an offset of the KBR antenna phase center for each satellite A and B ($\delta\rho_{APC}$):

$$\rho_{KBR1B} = \rho + \delta\rho_{SO} + \delta\rho_{APC_A} + \delta\rho_{APC_B} + \Delta\rho_{KBR1B}$$

$$\dot{\rho}_{KBR1B} = \dot{\rho} + \delta\dot{\rho}_{SO} + \delta\dot{\rho}_{APC_A} + \delta\dot{\rho}_{APC_B}$$

10    $$\ddot{\rho}_{KBR1B} = \ddot{\rho} + \delta\ddot{\rho}_{SO} + \delta\ddot{\rho}_{APC_A} + \delta\ddot{\rho}_{APC_B} \tag{14}$$

In the following, these two error sources are described.

6.1   System and Oscillator Noise

The following ASD model was used to generate KBR noise:

$$\tilde{\delta}\rho_{SO}(f) = 10^{-6} \cdot \sqrt{1 + \left(\frac{0.0018\text{Hz}}{f}\right)^4} \; \frac{\text{m}}{\sqrt{\text{Hz}}} \qquad 10^{-5} \le f \le 10^{-1} \tag{15}$$

15   This ASD model is in agreement with the system and oscillator KBR noise for the satellite pair separation of 238 km in Kim (2000). ~~Figure~~ Fig. 8 illustrates the ASD model. Based on this model, one month time series of the range noise was generated. Then numerical differentiation was used to generate range rate noise and range acceleration noise from the range noise time series (cf. Fig. 9).

6.2   Antenna Phase Center Pointing Jitter Coupling

20   The KBR instrument measures the distance between the antenna phase centers, which are placed nominally on the SF x-axis, almost 1.5 m away from the satellites' CoM. However, due to manufacturing imperfections and due to the large acceleration of the system during launch, the actual positions differ from the nominal ones. Consequently, any pointing jitter (deviations of the satellites' attitudes from their nominal attitudes) causes a geometric error in the ranging measurement. In the absence of such misplacements and in the absence of pointing jitter, this effect would be zero (rather, constant) and hence not effect the

25   measured (biased) range. Given the antenna phase center (APC) offset vector ($\boldsymbol{p}_A^{SF}$) in SF and the matrix rotating from SF to ICRF, this error is computed as:

$$\delta\rho_{APC_A} = -\left(\boldsymbol{e}_{AB}^{ICRF}\right)^T \cdot \mathbf{R}_{SF}^{ICRF} \cdot \boldsymbol{p}_A^{SF}, \tag{16}$$
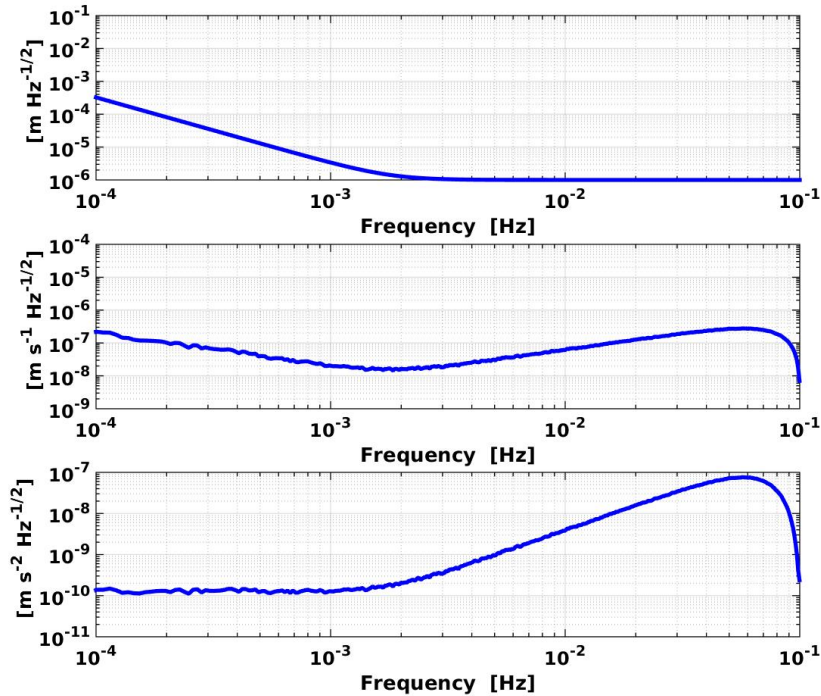
Figure 8. ASD of KBR ~~oscillator and~~ system and oscillator noise for range (top), range rate (middle) and range acceleration (bottom)

i.e. it is the APC offset (w.r.t. CoM) projected onto the line-of-sight. For the simulation, the $\mathbf{R}_{SF}^{ICRF}$ was calculated from equation (B1) using the error-free simulated quaternions, and the line-of-sight vector (e_{AB}^{ICRF}) was calculated from the error-free satellite positions in ICRF:

$$e_{AB}^{ICRF} = \frac{\boldsymbol{r}_B - \boldsymbol{r}_A}{|\boldsymbol{r}_B - \boldsymbol{r}_A|} \tag{17}$$

5   For GRACE-FO B, the indices A and B should be swapped in equations (16) and (17). ~~Figure~~ Fig. 10 shows time series of the APC offset pointing jitter coupling for one month of GRACE-FO A.

     In GRACE, there have been calibration manoeuvers in order to try and estimate the APC offset vectors ($\boldsymbol{p}_A^{SF}, \boldsymbol{p}_B^{SF}$). The estimates have been published by JPL in the VKB1B files (Case et al., 2002). For the simulations, values of similar magnitude
10   were chosen. These values are not directly given to the user, however, the simulated KBR1B files include a column of simulated estimated correction terms. This means that it is computed from the imperfect attitude information that is provided via simulated SCA1B files. Real GRACE KBR1B data also contains this column, which is called antenna offset correction (AOC) term (cf.
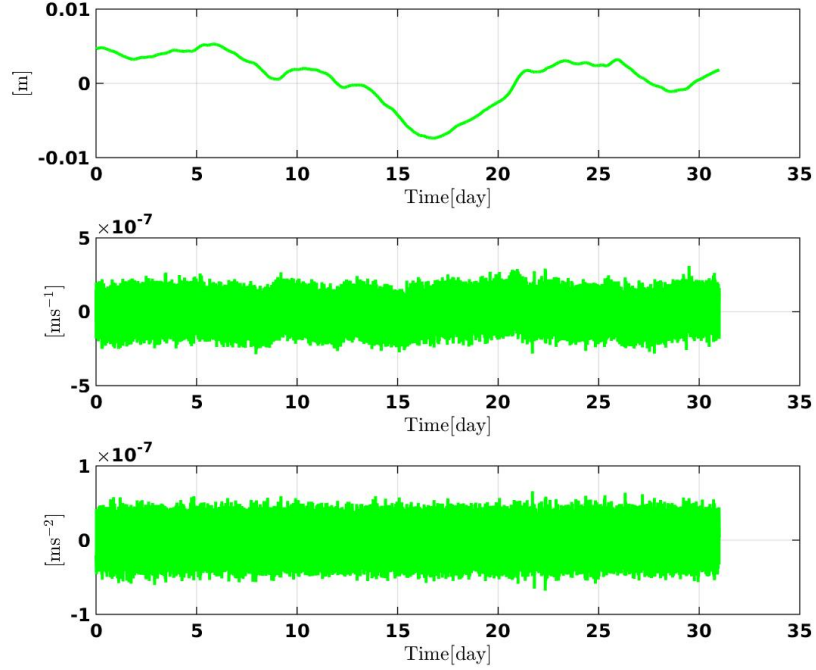
Figure 9. Time series of KBR oscillator and system noise for range (top), range rate (middle) and range acceleration (bottom)

Case et al., 2002) . It has to be added to the KBR ranging measurement, so it describes the negative of the error term:

$$AOC_\rho \approx -\delta\rho_{APC_A} - \delta\rho_{APC_B}. \tag{18}$$

For the simulations, the correction term of AOC_ρ was computed according to equation (16), with the difference that the matrix $\mathbf{R}_{SF}^{ICRF}$ was derived from the simulated noisy quaternions without the bias.

5   A second and third column is also provided, computed by numerical differentiation, describing the correction for range rate and range acceleration:

$$AOC_{\dot\rho} \approx -\delta\dot\rho_{APC_A} - \delta\dot\rho_{APC_B}$$
$$AOC_{\ddot\rho} \approx -\delta\ddot\rho_{APC_A} - \delta\ddot\rho_{APC_B}. \tag{19}$$
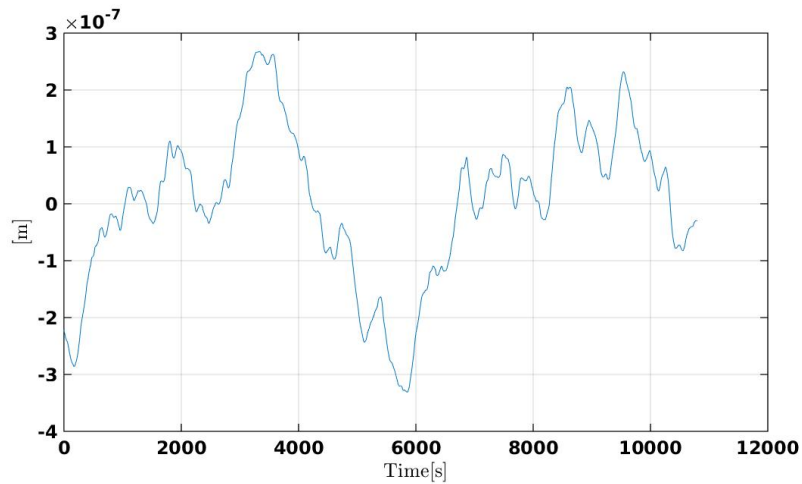
15

Figure 10. Time series of APC offset pointing jitter coupling with subtracted mean value, during two orbital revolutions for GRACE-FO A
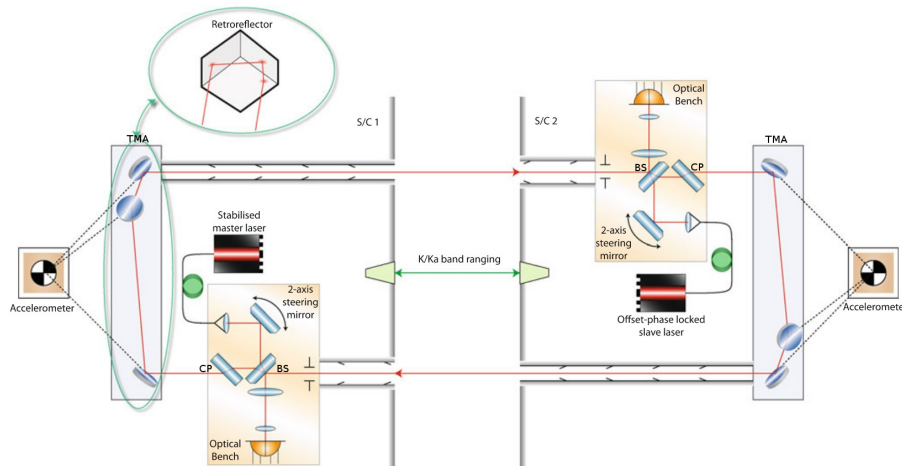

Figure 11. GRACE-FO laser ranging instrument optical layout (from Sheard et al. (2012)). BS beamsplitter, CP compensation plate, TMA triple mirror assembly

7 Simulating LRI1B Data

The structure of the LRI1B data file is similar to the KBR1B file, but it contains two additional observations of pitch and yaw angles. Tables D1 and D2 in Appendix D show the format of the data records for simulated KBR1B and LRI1B files. The simulated error-free range, range rate and range accelerations are calculated from the equations (11), (12) and (13). Apart from

a bias of a few centimeters, various other errors were added:

$$\rho_{LRI1B} = \alpha \cdot (\rho + \delta\rho_{LF} + \delta\rho_{TMA_A} + \delta\rho_{TMA_B} + \delta\rho_{ALQ_A} + \delta\rho_{ALQ_B} + \Delta\rho_{LRI1B})$$

$$\dot{\rho}_{LRI1B} = \alpha \cdot (\dot{\rho} + \delta\dot{\rho}_{LF} + \delta\dot{\rho}_{TMA_A} + \delta\dot{\rho}_{TMA_B} + \delta\dot{\rho}_{ALQ_A} + \delta\dot{\rho}_{ALQ_B})$$

$$\ddot{\rho}_{LRI1B} = \alpha \cdot (\ddot{\rho} + \delta\ddot{\rho}_{LF} + \delta\ddot{\rho}_{TMA_A} + \delta\ddot{\rho}_{TMA_B} + \delta\ddot{\rho}_{ALQ_A} + \delta\ddot{\rho}_{ALQ_B}) \tag{20}$$

In equations (20), $\alpha = 1 + 10^{-6}$ is a scale factor which is due to the limited accuracy of the absolute laser frequency value for the phase to length conversion. Three main LRI noise sources in equations (20) are: laser frequency (LF) noise ($\delta\rho_{LF}$), and the coupling of the pointing jitter into the length measurement via triple mirror assembly (TMA) (Fig. 11) for each satellite A and B ($\delta\rho_{TMA}$) and the additional linear and quadratic pointing jitter coupling ($\delta\rho_{ALQ}$). This is a selection of relatively well-known LRI error sources, where LF and TMA errors are expected to be the dominating ones. For the range rate and range acceleration noise, the errors were numerically differentiated. In the following, the LRI error sources are described in detail.
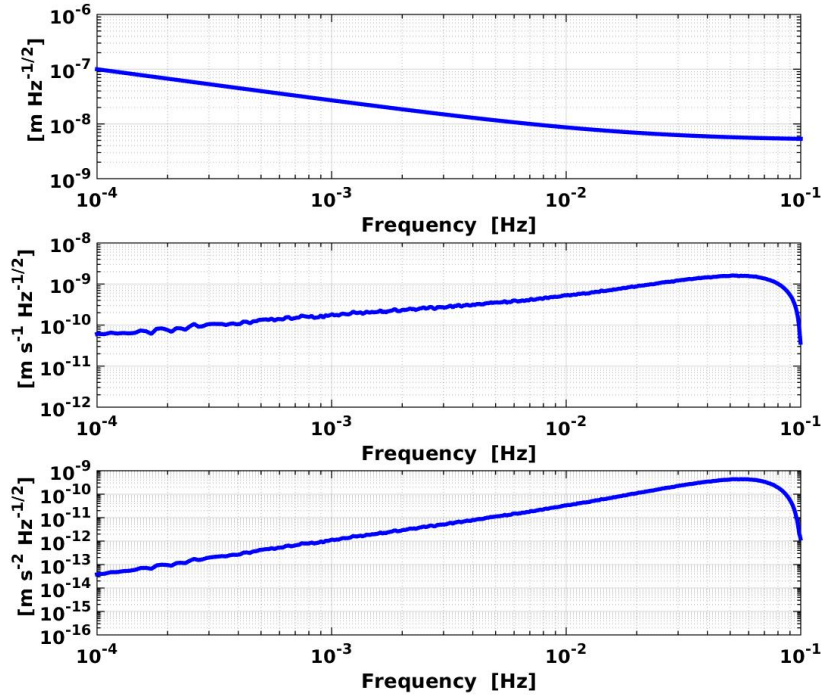

Figure 12. ASD of laser frequency noise for range (top), range rate (middle) and range acceleration (bottom)

17

7.1 Laser Frequency Noise

Based on LRI cavity performance tests carried out by JPL, the current best estimate of the ASD of the laser frequency noise (i.e., the ranging noise which is induced by frequency jitter of the LRI master laser) for a satellite separation of 238 km is:

$$\tilde{\delta}\rho_{LF}(f) = 5 \cdot 10^{-9} \cdot \sqrt{1 + \left(\frac{0.0182\text{Hz}}{f}\right)^2} \; \frac{\text{m}}{\sqrt{\text{Hz}}} \tag{21}$$

5 ~~Figure~~ Fig. 12 illustrates this noise. Note that this specific ASD corresponds to a constant satellite separation (of 238 km), which is a sufficient simplification for the purpose of generating noise time series.

One month time series of the range noise $\delta\rho_{LF}$ was generated from the ASD model (cf. Fig. 12). Then numerical differentiation was used to generate range rate noise and range acceleration noise from the noise range time series (cf. Fig. 13).
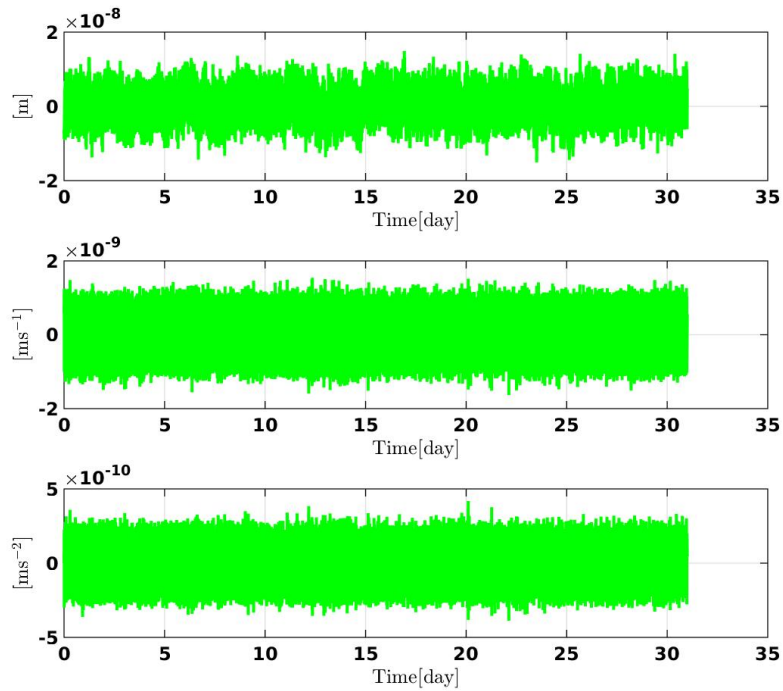

Figure 13. Time series of laser frequency noise for range (top), range rate (middle) and range acceleration (bottom)

7.2 Triple Mirror Assembly Pointing Jitter Coupling

With a good approximation, the LRI measures the biased distance between the TMA vertices of the twin satellites (Fig. 11). Both the pointing jitter and frame misalignments couple into the LRI ranging measurement. This effect is in principal the same as the geometric error effect due to the APC position in the KBR measurement. The only difference is that the nominal positions of the TMA vertices lie in the CoM, whereas the nominal positions of the APC are almost 1.5 m in SF-x-direction away from this point.
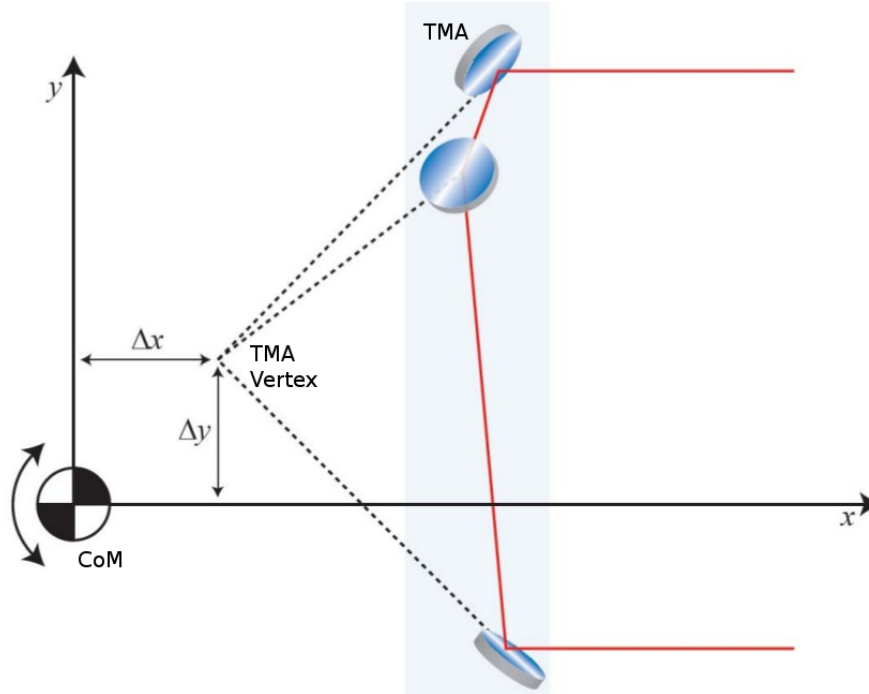

Figure 14. Triple mirror assembly vertex offset from the satellites' center of mass in two dimensions

An offset of the TMA vertex from the satellites'CoM leads to the coupling of satellite pointing jitter into the round trip length variations measured by the LRI (Fig. 14). The magnitudes of TMA vertex offset vectors (v^{SF}) along x, y and z axes were chosen in the order of a few hundred micrometers. The real values after the GRACE-FO launch are unknown and will have to be calibrated. To calculate $\delta\rho_{TMA}$, the TMA vertex offset vector (v^{SF}) is rotated from the SF into the ICRF and then projected onto the line-of-sight:

$$\delta\rho_{TMA_A} = -\left(e_{AB}^{ICRF}\right)^T \cdot \mathbf{R}_{SF}^{ICRF} \cdot v_A^{SF} \tag{22}$$

where e_{AB}^{ICRF} is the line-of-sight vector in ICRF. Again, for GRACE-FO B, indices A and B should be swapped. ~~Figure~~ Fig. 15 shows time series of TMA pointing jitter coupling for one month of GRACE-FO A.

Similar to the KBR1B files, LRI1B files contain correction terms - vertex point correction (VPC) terms - for range, range rate and range acceleration, which were calculated using the simulated noisy quaternions without the bias:

$$VPC_\rho \approx -\delta\rho_{TMA_A} - \delta\rho_{TMA_B}$$
$$VPC_{\dot\rho} \approx -\delta\dot\rho_{TMA_A} - \delta\dot\rho_{TMA_B}$$
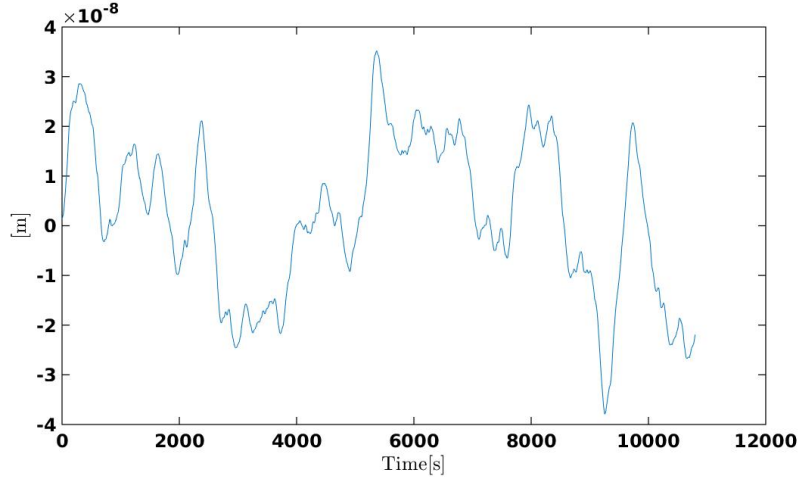$$VPC_{\ddot\rho} \approx -\delta\ddot\rho_{TMA_A} - \delta\ddot\rho_{TMA_B}. \tag{23}$$

Figure 15. Time series of TMA pointing jitter coupling with subtracted mean value, during two orbital revolutions for GRACE-FO A

7.3 Additional Linear and Quadratic Pointing Jitter Coupling

5   There is additional linear and quadratic coupling (ALQ) of the pointing jitter angles (θ_x, θ_y and θ_z) into the length measurements, which can be described as:

$$\delta\rho_{ALQ_A} = \begin{bmatrix} c_{x_A} & c_{y_A} & c_{z_A} \end{bmatrix} \cdot \begin{bmatrix} \theta_{x_A} \\ \theta_{y_A} \\ \theta_{z_A} \end{bmatrix} + \begin{bmatrix} \theta_{x_A} & \theta_{y_A} & \theta_{z_A} \end{bmatrix} \cdot \begin{bmatrix} c_{xx_A} & c_{xy_A} & c_{xz_A} \\ 0 & c_{yy_A} & c_{yz_A} \\ 0 & 0 & c_{zz_A} \end{bmatrix} \cdot \begin{bmatrix} \theta_{x_A} \\ \theta_{y_A} \\ \theta_{z_A} \end{bmatrix} \tag{24}$$

For GRACE-FO B, the indices A should be exchanged into B in equation (24). Linear coefficients of c_x, c_y and c_z are estimated to be in the order of a few $\frac{\mu m}{rad}$ and quadratic coefficients of c_{xy}, c_{xz} and ... are in the order of a few $\frac{mm}{rad^2}$. Error-free time series 10 of $\theta_x, \theta_y, \theta_z$ were used to simulate $\delta\rho_{ALQ}$. ~~Figure~~ Fig. 16 shows time series of ALQ pointing jitter coupling for one month of GRACE-FO A.
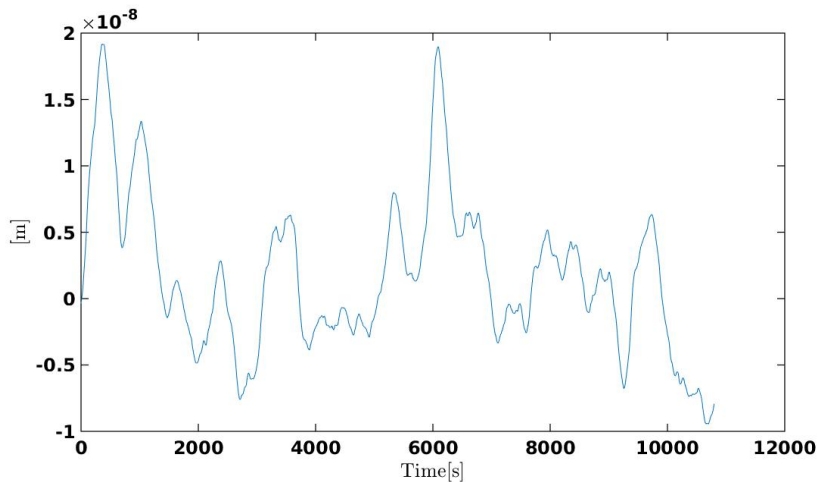
Figure 16. Time series of ALQ pointing jitter coupling with subtracted mean value, during two orbital revolutions for GRACE-FO A

7.4 Differential Wavefront Sensing: Pitch And Yaw Measurements

Differential wavefront sensing (DWS) is a well known technique for measuring the relative wavefront misalignment between two laser beams with high sensitivity (Sheard et al., 2012). ~~Figure~~ Fig. 17 illustrates the basic principal of DWS. DWS provides two extra measurements of the satellite attitude: yaw and pitch pointing angles with respect to the line-of-sight.

5

DWS angle measurements on board GRACE-FO are obtained from the steering mirror on the LRI optical bench (Sheard et al., 2012). The steering mirror orientation is controlled using the DWS error signals, constantly driving the error signals back to zero. The steering mirror orientation is recorded as pitch and yaw angles. However, the steering mirror can only turn in ~~quanta~~ discrete units of 4.5μrad around the pitch axis and 6μrad around the yaw axis. Therefore, the angle determination is 10 ~~quantization limited~~ limited to integer multiples of these units.
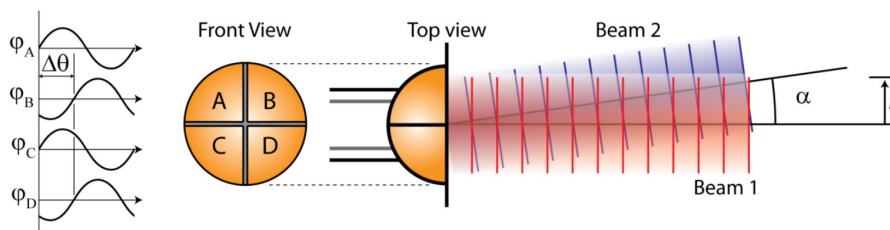

Figure 17. Differential wavefront sensing principal. Two beams of radius r with a relative wavefront tilt of α are detected by a quadrant photodetector. The two beams also have a slight frequency difference (from Sheard et al. (2012))

21

For each satellite, DWS pitch and yaw measurements were simulated by:

$$\theta_{y,DWS} = \text{round}\left(\frac{\theta_y}{4.5 \cdot 10^{-6}\text{rad}}\right) \cdot 4.5 \cdot 10^{-6}\text{rad} + \Delta\theta_{y,DWS}$$

$$\theta_{z,DWS} = \text{round}\left(\frac{\theta_z}{6.0 \cdot 10^{-6}\text{rad}}\right) \cdot 6.0 \cdot 10^{-6}\text{rad} + \Delta\theta_{y,DWS}, \tag{25}$$

where "round" means rounding towards nearest integer. $\theta_{y,DWS}$ and $\theta_{z,DWS}$ are the simulated DWS pitch and yaw angles, and θ_y and θ_z are the error-free pitch and yaw angles. The biases ($\Delta\theta_{y,DWS}$, $\Delta\theta_{y,DWS}$) stem mainly from a misalignment of the LRI frame with respect to the SF, which is expected to be within the range of few milliradians. ~~Figure~~ Fig. 18 shows simulated DWS pitch and yaw angles.
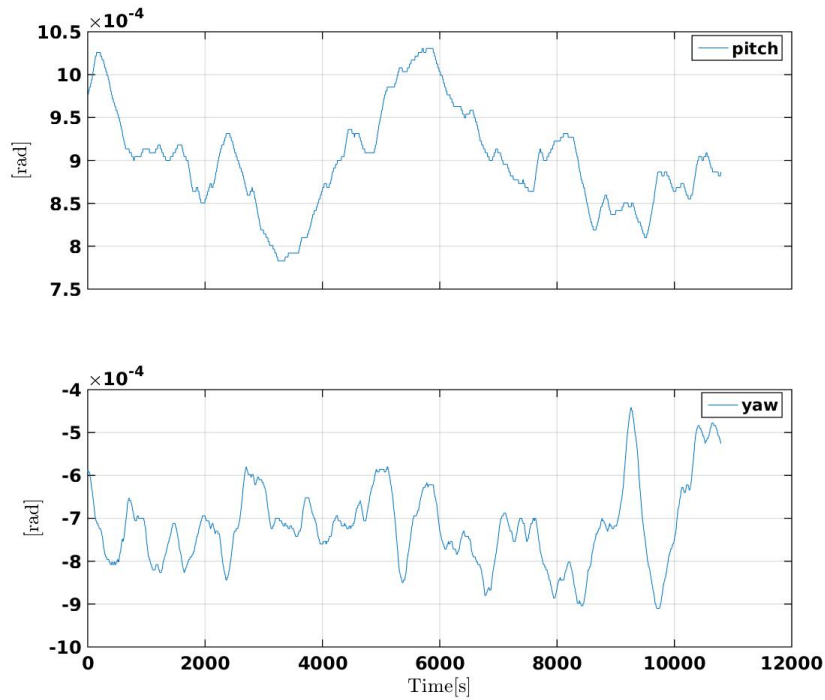

Figure 18. Simulated DWS pitch and yaw angles during two orbital revolutions for GRACE-FO A

8 Conclusions

~~The quality of the temporal gravity field solutions from the~~ We have described the simulation of observation and noise models for GRACE-FO ~~mission depends on its~~ multi-sensor system, consisting of inter-satellite ranging with microwave and laser ranging instrument, GPS orbit tracking, accelerometry, and attitude sensing. ~~In this paper, the simulation of observations and the noise models for GRACE-FO major instruments were described.~~ For the first time, simulated LRI data that includes DWS attitude information were generated. The simulated LRI ranging and attitude data may be used in different data analysis scenarios for GRACE-FO, such as combination of KBR and LRI data, calibration, or estimation of geometric corrections for both KBR and LRI ranging.

On the other hand, different Earth's gravity field solutions derived from actual satellite data can only be compared against each other, because the real Earth's gravity field is not known. This is a major problem in the evaluation of the performance of gravity field recovery approaches. A closed-loop simulation starting with a known gravity field provides the opportunity to overcome this problem by comparing the input gravity field and the gravity field solutions. Also, the effect of instrument noise on gravity field solutions can be investigated by comparing observation residuals with the simulated instrument noise.

Data availability. The simulated instrument GRACE-FO data are available via https://doi.org/10.22027/AMDC2.

Appendix A

In the following, we briefly describe the models for atmospheric drag and solar radiation pressure, that were used for the orbit simulations.

A1 Atmospheric Drag Model

The acceleration due to atmospheric drag is calculated with the following formula from aerodynamic theory (e.g., Montenbruck and Gill, 2000, p. 84), with A the satellite's cross sectional area, m the mass of the satellite, e_v the unit vector of the velocity relative to the atmosphere, C_D the drag coefficient and p the atmospheric density at the location of the satellite:

$$\ddot{r} = -\frac{1}{2} C_D \frac{A}{m} p v_r^2 \cdot e_v \tag{A1}$$

For the calculation of the relative velocity v_r, the assumption is made that the atmosphere co-rotates with the Earth. This leads to:

$$v_r = \dot{r} - \omega_\oplus \times r,$$

with $\dot{r}$ the inertial velocity vector of the satellite, r the position vector and $\omega_\oplus$ the Earth's angular velocity. v_r^2 in formula A1 is then the square of the absolute relative velocity,

$$v_r^2 = |v_r|^2.$$

A2 Solar Radiation Pressure Model

A satellite exposed to radiation from the Sun experiences a force arising from the absorption and reflection of incident photons. The resulting acceleration was modelled by:

$$\ddot{\boldsymbol{r}} = -\nu \frac{P_\odot}{m} \left(\frac{AU}{x} \right)^2 \cdot \sum_i \left[\cos(\alpha_i) A_i \cdot ((1 - \zeta_i) \cdot \boldsymbol{e} + 2\zeta_i \cos(\alpha_i) \cdot \boldsymbol{n}_i) \right]$$

$$= -\nu \frac{P_\odot}{m} \left(\frac{AU}{x} \right)^2 \cdot \sum_i \left[\langle \boldsymbol{n}_i, \boldsymbol{e} \rangle A_i \cdot ((1 - \zeta_i) \cdot \boldsymbol{e} + 2\zeta_i \langle \boldsymbol{n}_i, \boldsymbol{e} \rangle \cdot \boldsymbol{n}_i) \right], \tag{A2}$$

5   where the sum is to be taken over all satellite surfaces i that are illuminated by the sunlight, i.e. over all surfaces i such that

$$\cos(\alpha_i) = \langle \boldsymbol{n}_i, \boldsymbol{e} \rangle > 0. \tag{A3}$$

Here, α_i is the angle of incidence, $\boldsymbol{n}_i$ is the outward pointing normal vector to the surface i, and $\boldsymbol{e}$ is the normalized vector pointing from the satellite's CoM towards the Sun. x is the Sun-satellite distance, A_i is the area of the surface i, so that $\cos(\alpha_i) A_i$ is its cross-sectional part. The ζ_i are the reflection coefficients of the respective surfaces, combining reflection co-

10 efficients for visible and IR light. $P_\odot$ denotes the solar radiation pressure at 1 AU (Astronomical Unit) distance from the Sun, with a flux (pressure times speed of light) amounting to about $1367 \mathrm{Wm}^{-2}$. The left term under the sum in equation A2 accounts for the absorbed photons and the right term accounts for the photon reflections. The shadow function ν is a value between 0 (in shadow) and 1 (fully illuminated), calculated using a geometric shadow model with umbra and penumbra cones, ignoring atmosphere and flattening of the Earth. For more details look at Montenbruck and Gill (2000).

15

In the above equations, the total mass for each GRACE-FO satellite is $m = 655 \mathrm{kg}$. A GRACE-FO satellite weighs about 180kg more than a GRACE satellite, due to the additional payload (Gath, 2016).

Appendix B

There are several possible definitions of the pointing angles. However, if the rotation direction is clear, the different methods

20 differ only in the second order. I.e., the differences are in the order of microradians, at most, which can be considered negligible with respect to the measurement uncertainty.

Inter-satellite pointing can be geometrically interpreted as deviations of the SF from the LOSF (Bandikova et al., 2012). Pointing jitter or variations can be expressed as a sequence of rotations about the roll (i.e., $\boldsymbol{x}_{LOSF}$), pitch (i.e., $\boldsymbol{y}_{LOSF}$) and yaw (i.e., $\boldsymbol{z}_{LOSF}$) axes. The roll, pitch and yaw angles can be derived from the matrix rotating from SF to LOSF (cf. Fig. 1).

The matrix rotating from SF to ICRF is related to the quaternions by (Wu et al., 2006):

$$
\mathbf{R}_{SF}^{ICRF} =
\begin{bmatrix}
q_0^2 + q_1^2 - q_2^2 - q_3^2 & 2(q_1 q_2 - q_0 q_3) & 2(q_1 q_3 + q_0 q_2) \\[2mm]
2(q_1 q_2 + q_0 q_3) & q_0^2 - q_1^2 + q_2^2 - q_3^2 & 2(q_2 q_3 - q_0 q_1) \\[2mm]
2(q_1 q_3 - q_0 q_2) & 2(q_2 q_3 + q_0 q_1) & q_0^2 - q_1^2 - q_2^2 + q_3^2
\end{bmatrix}
\tag{B1}
$$

Here, q are the quaternions mentioned in section 4.

The matrix rotating from ICRF to LOSF is derived from the orbital positions:

$$
\mathbf{R}_{ICRF}^{LOSF} = [\boldsymbol{x}_{LOSF} \ \boldsymbol{y}_{LOSF} \ \boldsymbol{z}_{LOSF}],
\tag{B2}
$$

with the LOSF axes are column vectors according to the definition in section 2, expressed in inertial frame. Then, the pointing angles (roll θ_x, pitch θ_y and yaw θ_z) can be computed from the rotation matrix $\mathbf{R}_{SF}^{LOSF} = \mathbf{R}_{ICRF}^{LOSF} \cdot \mathbf{R}_{SF}^{ICRF}$ by:

$$
\theta_x = \arctan\left(\frac{R_{32}}{R_{33}}\right)
$$

$$
\theta_y = -\arcsin\left(R_{31}\right)
$$

$$
\theta_z = \arctan\left(\frac{R_{21}}{R_{11}}\right)
\tag{B3}
$$

where R_{ij} are the elements of $\mathbf{R}_{SF}^{LOSF}$. Here, the first index refers to the row and the second index refers to the column.

Appendix C

The following is a numerically stable pseudocode to compute quaternions from a given rotation matrix, where R denotes the rotation matrix and R(i,j) its element in the ith row and j[th] column.

```
IF ( R(1,1) >= R(2,2) AND R(1,1) >= R(3,3) )

r = sqrt(1 + R(1,1) - R(2,2) - R(3,3));
s = 1/(2*r);
q0 = (R(3,2)-R(2,3))*s;
q1 = r/2;
q2 = (R(2,1)+R(1,2))*s;
q3 = (R(1,3)+R(3,1))*s;
```

25

```
     ELSEIF ( R(2,2) > R(1,1) AND R(2,2) >= R(3,3) )


     r = sqrt(1 + R(2,2) - R(1,1) - R(3,3));
     s = 1/(2*r);
 5   q0 = (R(1,3)-R(3,1))*s;
     q1 = (R(1,2)+R(2,1))*s;
     q2 = r/2;
     q3 = (R(3,2)+R(2,3))*s;


10   ELSE


     r = sqrt(1 + R(3,3) - R(1,1) - R(2,2));
     s = 1/(2*r);
     q0 = (R(2,1)-R(1,2))*s;
15   q1 = (R(1,3)+R(3,1))*s;
     q2 = (R(2,3)+R(3,2))*s;
     q3 = r/2;


     END
20
```

Appendix D

Tables D1 and D2 describe the format of the data records for KBR1B and LRI1B simulated files. For the consistency we kept the tables similar to Case et al. (2002).

Table D1. KBR Data Format Record (KBR1B)

Parameter	Definition	Format	Units
gps_time	GPS time, seconds past 12:00:00, noon 01-Jan-2000	9 i	s
range	Range between GRACE A and B	16.10 f	m
range_rate	Range rate between GRACE A and B	18.16 f	m/s
range_accl	Range acceleration between GRACE A and B	21.18 f	m/s^2
ioni_corr	Ionospheric range correction between GRACE A and B for Ka frequencies	16.15 f	m
lighttime_corr	Light time range correction between GRACE A and B	16.15 e	m
lighttime_rate	Light time range rate correction between GRACE A and B	16.15 e	m/s
lighttime_accl	Light time range acceleration correction between GRACE A and B	16.15 e	m/s^2
ant_centr_corr	Antenna phase center range correction	16.15 f	m
ant_centr_rate	Antenna phase center range rate correction	16.15 e	m/s
ant_centr_accl	Antenna phase center range acceleration correction	16.15 e	m/s^2
K_A_SNR	SNR K band for GRACE A	3 i	.1 db-Hz
Ka_A_SNR	SNR Ka band for GRACE A	3 i	.1 db-Hz
K_B_SNR	SNR K band for GRACE B	3 i	.1 db-Hz
Ka_B_SNR	SNR Ka band for GRACE B	3 i	.1 db-Hz
qualflg	0 = not Defined	0.8 i	N/A

Table D2. LRI Data Format Record (LRI1B)

Parameter	Definition	Format	Units
gps_time	GPS time, seconds past 12:00:00, noon 01-Jan-2000	9 i	s
range	Range between GRACE A and B	19.10 f	m
range_rate	Range rate between GRACE A and B	19.16 f	m/s
range_accl	Range acceleration between GRACE A and B	22.19 f	m/s^2
lighttime_corr	Light time range correction between GRACE A and B	16.15 e	m
lighttime_rate	Light time range rate correction between GRACE A and B	16.15 e	m/s
lighttime_accl	Light time range acceleration correction between GRACE A and B	16.15 e	m/s^2
ver_point_corr	Vertex point range correction	16.15 f	N/A
ver_point_rate	Vertex point range rate correction	16.15 e	m/s
ver_point_accl	Vertex point range acceleration correction	16.15 e	m/s^2
pitch_A_dws	Pitch angle from differential wavefront sensing for GRACE A	19.17 f	rad
yaw_A_dws	Yaw angle from differential wavefront sensing for GRACE A	19.17 f	rad
pitch_B_dws	Pitch angle from differential wavefront sensing for GRACE B	19.17 f	rad
yaw_B_dws	Yaw angle from differential wavefront sensing for GRACE B	19.17 f	rad
LRI_A_SNR	SNR LRI for GRACE A	3 i	.1 db-Hz
LRI_B_SNR	SNR LRI for GRACE B	3 i	.1 db-Hz
qualflg	0 = not Defined	0.8 i	N/A

References

Bandikova, T., Flury, J., and Ko, U.: Characteristics and accuracies of the GRACE inter-satellite pointing, Advances in Space Research, 50, 2012.

Case, K., Kruizinga, G., and Wu, S.: GRACE level 1B data product user handbook, JPL Publication D-22027, 2002.

5 Flechtner, F., Neumayer, K.-H., Dahle, C., Dobslaw, H., Fagiolini, E., Raimondo, J.-C., and Güntner, A.: What Can be Expected from the GRACE-FO Laser Ranging Interferometer for Earth Science Applications?, Surveys in Geophysics, 37, 453–470, doi:10.1007/s10712-015-9338-y, https://doi.org/10.1007/s10712-015-9338-y, 2016.

Franklin, J. N.: Numerical simulation of stationary and non-stationary gaussian random processes, SIAM Review, 7, 68–80, 1965.

Gath, P.: Integration und Test der GRACE Follow-On Satelliten, Tech. Rep. 420305, Deutscher Luft- und Raumfahrtkongress, 2016.

10 Gerlach, C., Földvary, L., Švehla, D., Gruber, T., Wermuth, M., Sneeuw, N., Frommknecht, B., Oberndorfer, H., Peters, T., Rothacher, M., Rummel, R., and Steigenberger, P.: A CHAMP-only gravity field model from kinematic orbits using the energy integral, Geophysical Research Letters, 30, 2003.

Harvey, N.: GRACE star camera noise, Advances in Space Research, 58, 2016.

Horwath, M., Lemoine, J., Biancale, R., and Bourgogne, S.: Improved GRACE science results after adjustment of geometric biases in the

15   Level-1B K-band ranging data, Journal of Geodesy, 85, 2011.

Kim, J.: Simulation study of a low-low satellite-to-satellite tracking mission, Ph.D. thesis, The University of Texas at Austin, 2000.

Mayer-Gürr, T.: Gravitationsfeldbestimmung aus der Analyse kurzer Bahnbögen am Beispiel der Satellitenmissionen CHAMP und GRACE, Ph.D. thesis, Universitäts-und Landesbibliothek Bonn, 2006.

Montenbruck, O. and Gill, E.: Satellite Orbits, "Springer-Verlag, "Berlin Heidelberg 2000, 2000.

20 Müller, V.: Orbit simulation Toolkit, Ph.D. thesis, Bachelor of Science Degree Thesis, Max-Planck-Institute for Gravitational Physics (Albert Einstein Institute, AEI) and Gottfried Wilhelm Leibniz Universtitut, Hannover, 2010.

Naeimi, M., Wegener, H., Darbeheshti, N., Mueller, V., Schnitger, A., Goswami, S., Flury, J., Hewitson, M., and Heinzel, G.: Instrument Data Simulations for GRACE Follow-on: Overview and Goals, Advances in Space Research, under review, 2017.

Petit, G. and Luzum, B.: IERS Conventions (2010), Tech. Rep. IERS Technical Note No. 36, Frankfurt am Main: Verlag des Bundesamts für

25   Kartographie und Geodäsie, 2010.

Reigber, C.: Gravity field recovery from satellite tracking data, in: Theory of satellite geodesy and gravity field determination, pp. 197–234, Springer, 1989.

Rieser, D., Mayer-Gürr, T., Savcenko, R., Bosch, W., Wünsch, J., Dahle, C., and Flechtner, F.: The ocean tide model EOT11a in spherical harmonics representation, Technical Note, 2012.

30 Rummel, R.: Determination of short-wavelength components of the gravity field from satellite-to-satellite tracking or satellite gradiometry-an attempt to an identification of problem areas, Manuscripta Geodaetica, 4, 107–148, 1979.

Sheard, B., Heinzel, G., Danzmann, K., Shaddock, A., Klipstein, W., and Folkner, W.: Intersatellite laser ranging instrument for the GRACE follow-on mission, J Geod, 86, 1083–1095, 2012.

Standish, E. M.: JPL Planetary and Lunar Ephemerides, DE405/LE405, Jet Propulsion Laboratory Interoffice Memorandum, IOM 312.F -

35   98 - 048, 1998.

Stanton, R., Bettadpur, S., Dunn, C., Renner, K.-P., and Watkins, M.: Gravity Recovery And Climate Experiment (GRACE) science & mission requirements document, 1998.

Tapley, B. D., Bettadpur, S., Watkins, M., and Reigber, C.: The gravity recovery and climate experiment: Mission overview and early results, Geophysical Research Letters, 31, n/a–n/a, doi:10.1029/2004GL019920, http://dx.doi.org/10.1029/2004GL019920, l09607, 2004.

Wahr, J., Molenaar, M., and Bryan, F.: Time variability of the Earth's gravity field: Hydrological and oceanic effects and their possible detection using GRACE, Journal of Geophysical Research: Solid Earth, 103, 30 205–30 229, doi:10.1029/98JB02844, http://dx.doi.org/10.1029/98JB02844, 1998.

Watkins, M., Flechtner, F., Webb, F., Landerer, F., and Grunwald, L.: Current Status of the GRACE Follow-On Mission, Presented at the European Geosciences Union General Assembly, Vienna , Austria, 2016.

Wu, S.-C., Kruizinga, G., and Bertiger, W.: Algorithm theoretical basis document for GRACE level-1B data processing V1. 2, 2006.